Modality maps within primate somatosensory cortex

Robert M. Friedman*†, Li Min Chen‡, and Anna Wang Roe‡

Departments of ‡Neurobiology and *Anesthesiology, Yale University School of Medicine, New Haven, CT 06520-8051

Communicated by Jon H. Kaas, Vanderbilt University, Nashville, TN, July 7, 2004 (received for review April 1, 2004)

The sensations of pressure, flutter, and vibration are psychophysically distinct tactile modalities produced by frequency-specific vibrotactile stimulation of different mechanoreceptors in the skin. The information coded by the different low-threshold mechanoreceptors are carried by anatomically and electrophysiologically distinct pathways that remain separate at least up to and including the input stage of primary somatosensory cortex (SI) in primates, area 3b. Little is known about the functional organization of tactile representation beyond that stage. By using intrinsic optical imaging methods to record from area 1, the second processing stage of SI, we present evidence that pressure, flutter, and vibratory stimuli activate spatially distinct cortical domains in area 1, further strengthening the foundation for modality-specific processing streams in SI. These modality domains exhibit an organization that is unlike the discontinuous modality maps in visual area V2 but more like the continuous visual orientation maps in V1. The results demonstrate that psychophysically distinct sensory modalities can have fundamentally different modes of cortical representation.

The representation of visual features in early visual cortical pathways is reasonably well characterized, but how stimulus features are represented for the other senses is largely unknown. Within each retinotopic domain in area V1, the first visual cortical area, color is mapped discontinuously in domains called blobs, whereas orientation is mapped continuously and is characterized by a pinwheel organization (1, 2). In contrast, in the second visual cortical area, area V2, the visual submodalities of color, form, and depth are represented in large stripes (termed the thin pale stripes and thick stripes, respectively) (3), leading to three separate interdigitating topographic maps of visual space, each of which is discontinuous in nature (4). Thus, different visual cortical areas can map similar features in different manners. In somatosensory cortical areas, responses of individual neurons to the features of tactile objects have been characterized (5–12); however, little is known as to whether there are functional cortical maps representing tactile features and whether such features would be mapped in a continuous or discontinuous manner.

For low-threshold vibrotactile stimuli, the distinct perceptions of pressure, flutter, and vibration have been linked to different psychophysical channels and different mechananoreceptors. Slowly adapting Merkel cells (SAs) are sensitive to low frequency stimulation (<10 Hz) and primarily encode the pressure, texture, and form of an object; rapidly adapting Meissner corpuscles (RAs) are most sensitive to vibrotactile frequencies of 30 Hz and respond to the flutter, slip, and motion of objects; and Pacinian corpuscles (PCs) are most sensitive to high-frequency vibrations centered around 200 Hz (13–16). The precise role of Ruffini endings, which are found in the glabrous skin of humans but lacking in non-human primates, is unclear. In everyday haptic touch, the vibrotactile channels are simultaneously activated during the identification and manipulation of tactile objects.

Vibrotactile information is carried by anatomically and electrophysiologically distinct pathways from the periphery (17, 18). In area 3b, the first stage of primary somatosensory cortex (SI) processing, evidence indicates the presence of segregated modality domains for input provided by SA and RA mechanoreceptors (19–22); however, it is entirely unknown whether such segregation exists at stages beyond area 3b. What is known is that in SI, focal electrical stimulation can elicit modality-specific perception (e.g., of flutter) (23, 24). These tactile percepts remain distinct even during tasks that require higher cortical processing and involve discrimination, learning, and memory (25). These studies thus suggest the maintenance of at least some degree of segregated processing at higher cortical levels.

In this paper, we focus on the next hierarchical stage of processing in SI, area 1. Area 1 bears a close anatomical, physiological, and topographic relationship with area 3b (26–28) but is distinguished from area 3b by neurons with complex receptive fields that integrate information over large spatial extents (7, 8). Here, we address two issues. First, we ask whether area 1 processes different classes of vibrotactile inputs in segregated domains. Second, we examine possible parallels between somatosensory and visual processing. Because both areas 1 and V2 are considered second stages of cortical processing (cf. 28), we are interested in whether the functional organizations of areas 1 and V2 bear any similarities. V2 contains segregated domains (stripes) representing the visual modalities of color, form, and ocular disparity; these three domains are topographically discontinuous and interleaved (4). To our knowledge, whether such organization exists in area 1 has not previously been examined. Here, we report the presence of modality-specific pressure, flutter, and vibration domains in area 1 and describe an organization that differs from modality-specific functional architectures in visual cortex.

Methods

Surgical Procedures. We used conventional intrinsic optical imaging methods and single-unit recordings to map responses to fingerpad stimulation in three adult squirrel monkeys anesthetized with isoflurane (1–1.5%) (19). A craniotomy and durotomy exposed anterior parietal cortex. Before imaging, a brief electrophysiological recording session was performed to map the fingerpad regions of areas 3b and 1. Experiments were performed under protocols approved by the Yale Animal Care and Use Committee.

Finger Stimulation. Modality-specific cortical activity was mapped by stimulating the glabrous skin of a distal fingerpad with sinusoidal indentations. Fingers were secured in plasticine, leaving the glabrous surfaces available for tactile stimulation. A distal fingerpad (D2–D4) was stimulated with a round-tipped Teflon probe (3 mm in diameter) attached through an armature to a force-controlled torque motor (Aurora Scientific, Aurora, Canada). With the probe already loaded onto the skin (204-mN force), the distal fingerpad was stimulated in different trials with a 1-Hz (204-mN peak force, 450-μm peak-to-peak amplitude), 30-Hz (61.2 mN, 65 μm), or 200-Hz (16.3 mN, 12 μm) sinusoidal waveform of 4-sec duration, each known to elicit the different percepts of pressure (1 Hz), flutter (30 Hz), or vibration (200 Hz)

Freely available online through the PNAS open access option.

Abbreviations: SA, slowly adapting Merkel cell; RA, rapidly adapting Meissner corpuscle; PC, Pacinian corpuscle; SI, primary somatosensory cortex.

†To whom correspondence should be sent at the present address: Department of Psychology, Vanderbilt University, 301 Wilson Hall, 111 21st Avenue South, Nashville, TN 37203. E-mail: robert.friedman@vanderbilt.edu.

www.pnas.org/cgi/doi/10.1073/pnas.0404884101

in primates. The 30- and 200-Hz vibrotactile frequencies were chosen because the RA and PC mechanoreceptors show the lowest threshold for activation at these frequencies, respectively (15). With low-frequency stimulation (1 Hz) SA mechanoreceptors respond vigorously, whereas RA and PC mechanoreceptors do not (29). Thus, each stimulus was designed to preferentially activate one receptor type over the other two. These stimuli, although not selective, preferentially activated SA type I, RA type I, and PC type II mechanoreceptors, respectively. To optically map the topography of the fingerpads, stimuli consisted of a trapezoidal indentation (ramp rate = 25 msec; plateau duration = 4 s) with a peak compressional force of 306 mN and indentation of 790 μm.

Image Acquisition. Images were acquired through an optical chamber with an 8-bit video charge-coupled device camera using an Imager 2000 system (Optical Imaging, Germantown, NY), encoding differential signal, and 630-nm wavelength illumination. Vibrotactile stimuli were presented in a randomly interleaved manner in blocks consisting of five trials per stimulus type. For each condition, 40–50 trials were collected. Intrinsic image maps were collected at 15 image frames per sec for 3 sec starting 200 msec before stimulus onset. Interstimulus intervals were between 8–10 sec.

Image Analysis. For each stimulus condition, image frames 5–15 were summed to maximize the signal-to-noise ratio. To reduce blood vessel artifact we used blank subtraction for which the "blank" reference was a 3-sec image acquired during no stimulus presentation (blank condition). To delineate regions of strongest activation, images were low-pass filtered with a 4-pixel rectangular spatial filter and then thresholded at the top 15% of the gray pixel value distribution to identify regions of strongest activation. Boundaries of thresholded regions were determined and overlaid with the original optical maps and blood vessel maps for comparison. To confirm reliability and consistency of the signal, we evaluated the frame-to-frame temporal development of optical images and compared the similarity of images obtained by summing different blocks of trials (cf. 19).

Vector Analysis. The "vector" analysis was performed with custom-written software and was based on vector analysis developed for analyses of visual cortical orientation maps (30). In this analysis, response preference is represented by direction in color space (e.g., red for pressure, green for flutter, and blue for vibration) and magnitude is encoded by saturation of color. This method calculates, for each pixel, the relative weight of each response direction and gives a vector value that reflects the overall preferred direction and magnitude. More specifically, this method combines n images (where n is the number of different stimuli; in this case, $n = 3$) pixel by pixel (in an n-vector space), where the preferred response of each pixel is determined by the vector sum of the n directions. Each individual map was normalized so that each vector direction would contribute equally to the summed map. Pixels that exhibit strong response to only one stimulus will be dominated by a single color, where those with responses to multiple directions will have intermediate colors (see Fig. 2). Pixels that respond equally well to all stimuli will appear gray (where dark indicates low activation and bright indicates high activation).

Results

Sinusoidal indentations were used to elicit sensations of pressure (1 Hz), flutter (30 Hz), and vibration (200 Hz) (14, 15) on the glabrous distal fingerpads of anesthetized squirrel monkeys. Optical imaging was used to detect activity-related changes in cortical reflectance. Changes in reflectance (darkening of cortex) are associated with an elevation of neural activity. Fig. 1 illustrates the temporal development and spatial distribution of modality-specific (pressure, flutter, and vibration) cortical activity in SI revealed by optical imaging of intrinsic cortical signals. These raw response maps exhibited regions with large (dark pixels) and small (lighter pixels) reflectance changes. It is unlikely that these responses resulted from random fluctuations in cortical reflectance, because these images are the sum of 40 trials and are distinct from the blank condition (Fig. 1*Be*). Furthermore, consistent with known characteristics of the intrinsic signal, the signal developed gradually and consistently over a 3-sec period (Fig. 1*A*) and exhibited a reflectance amplitude change on the order of 0.1–1.0% (see Fig. 1*B k–m*).

Importantly, these activation patterns differed for the different vibrotactile stimuli. To visualize regions of strongest activation, methods common in studies of visual cortex were used (31). After low-pass filtering and thresholding of the pixel value distribution, we outlined the activations in red (pressure), green (flutter), and blue (vibration) (Fig. 1*B f–h*). These low-pass and threshold methods were used to accentuate loci of strongest activation, which are evident from inspection of the raw images, and show the distinctness of pressure, flutter, and vibration response. Akin to maps of somatosensory cortex observed with 2-deoxyglucose methodology (32) and thalamocortical projection patterns (33), these zones were discontinuous, had irregular shapes ranging from 200 to 1,000 μm in size, and were distributed across 2–3 mm of cortex.

Although single-condition maps illustrate all regions responsive to a particular stimulus, subtraction maps reveal preference for one stimulus over another. In the flutter–pressure (RA–SA) subtraction map, shown in Fig. 1*B d* and *i*, domains with a relative preference for flutter (black pixels) are interdigitated with domains with preference for pressure (white pixels). Such subtractions revealed organizational size and structure that were not evident in the single-condition maps in Fig. 1*B a–c*.

The selectivity of single cortical locations is further illustrated by examining the timecourse of optical response (Fig. 1*B k–m*). The magnitude of the response (defined as the peak change in reflectance) at each location is selective for the stimulus presented. For locations that fall squarely in only one domain type (locations indicated by a red diamond, green square, and blue triangle in Fig. 1*B f–h*), response amplitudes are maximally modulated by pressure (Fig. 1*Bk*), flutter (Fig. 1*Bl*), or vibration (Fig. 1*Bm*), respectively. Some locations (such as areas of red, blue, and green overlap in Fig. 1*Bj*) had mixed modal responses. Thus, the magnitude, stimulus specificity, temporal characteristics, and repeatability of the reflectance signal were consistent with the interpretation that the image patterns reflected stimulus-induced activity in area 1.

By using a vector summation method to determine a pixel-by-pixel, weighted response to the pressure, flutter, and vibration stimuli (methodology details are described in *Supporting Materials*, which is published as supporting information on the PNAS web site) we observed vibrotactile preference domains for each of the different fingerpads stimulated (n = 5 cases), in that clusters of pixels exhibited a saturated color that would be evident only if one vector magnitude dominated the other two. Three examples of such pixel-wise SA/RA/PC vector summation are illustrated in Fig. 2 *A–C Left*. Pixel locations with a dominant SA response appear bright red, those with a dominant RA response appear bright green, and those with a dominant PC response appear bright blue. Patches of cortex that are coded white indicate areas exhibiting strong response to each of the pressure, flutter, and vibratory stimuli. In each map, we observed an irregular, interdigitating pattern of pressure (red), flutter (green), and vibration (blue) domains interspersed in some maps with domains of mixed preference (e.g., light blue).

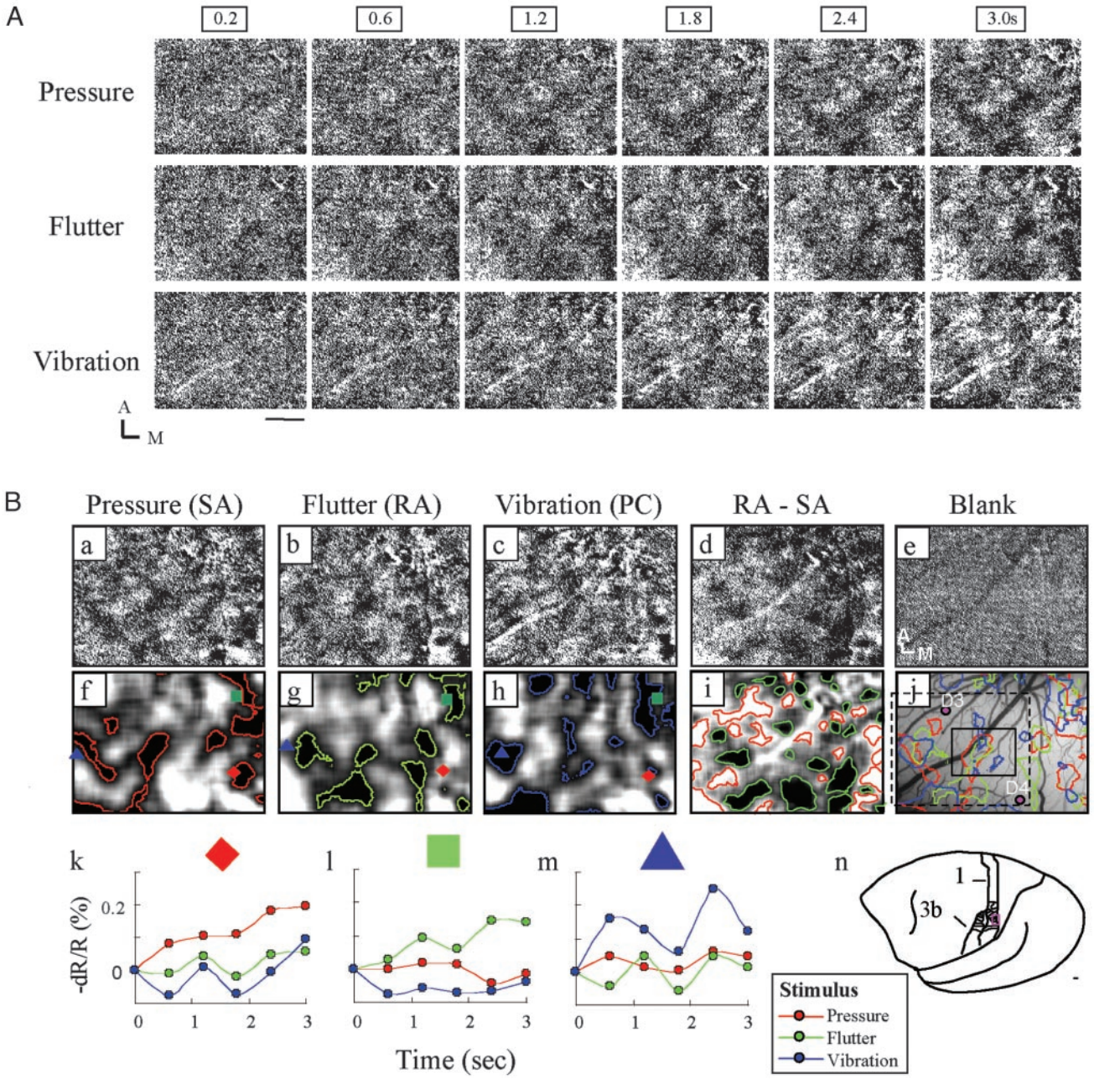

Fig. 1. Vibrotactile stimulation of D4 evokes modality-specific activation in area 1. (*A*) Temporal development and consistency of the intrinsic cortical response to pressure, flutter, and vibratory stimuli. Dark pixels indicate activation. For each stimulus, six images spanning 3 sec are shown (stimulus onset at frame 0.2 sec). (Scale bar, 1 mm.) A, anterior; M, medial. Data are the sum of 40 trials. (*B*) Single-condition blank-subtracted maps show modality-specific activation patterns. (*a–c*) Same as last images shown in *A* (3 sec). (*d* and *i*) Subtraction maps of flutter–pressure (RA–SA) illustrate irregular alternating dark (preference for flutter) and light (preference for pressure) domains (gray pixels indicate equal preference for both). (e) Blank condition map. (*f–i*) Activation outlines of *a–d* obtained by low-pass filtering and thresholding. The red diamond, green square, and blue triangle indicate sampled locations in *k–m*. (*j*) Blood vessel map with pressure, flutter, and vibration activation outlines superimposed. Sample electrode penetrations are indicated by labeled dots. The black box indicates the region shown in Fig. 3C. (*k–m*) Time courses of signal reflectance change illustrate modality-specific preference: pressure-dominant locus (red diamonds), flutter-dominant locus (green squares), and vibration-dominant locus (blue triangles). (*n*) Location of fingerpad representation in area 1 in the squirrel monkey (adapted from ref. 45). Small red box indicates area of imaging. Data are the sum of 40 trials. (Scale bar, 1 mm.)

Prior electrophysiological studies have not observed modular domains for vibrotactile stimuli in area 1 (7, 8). One possibility for this result is that the small patch size of the modular domains in area 1 revealed in our optical images would be difficult to discern solely with single and multiunit electrophysiology. In addition, prior studies focused on the adaptation (rapidly or slowly adapting) properties of neurons in area 1 rather than on whether the neurons were integrating information originating from SA, RA, or PC mechanoreceptors. When we examined these maps electrophysiologically, we found that, consistent with previous studies (8, 20), single electrophysiological penetrations contained a mixture of neurons with SA, RA, and/or PC responses and single neurons that contained mixed responses. Often, we recorded neurons with solely rapidly adapting responses or mixed slowly and rapidly adapting responses (Fig. 5*F*, which is published as supporting information on the PNAS web

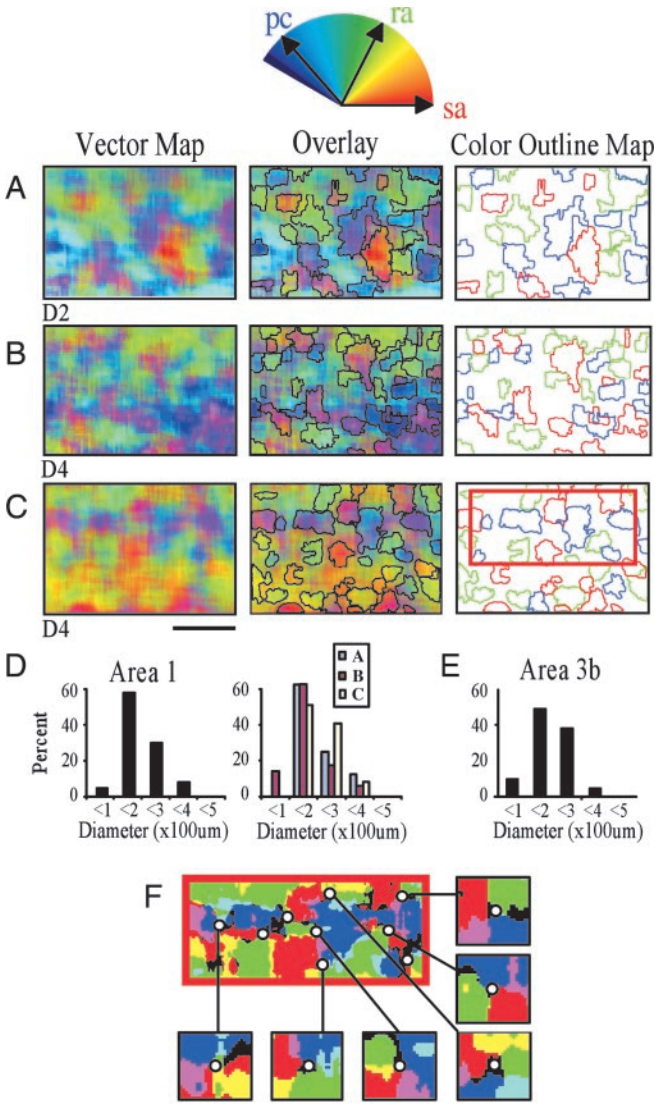

Fig. 2. Area 1 vector maps. Shown above *A* is the color-coded vector space. (*A–C*) Digits D2 (*A*), D4 (*B*), and D4 (*C*) were stimulated. (*Left*) Composite vector maps. Red, green, and blue indicate strong preference for pressure, flutter, and vibration, respectively. (*Center*) Vector maps with color threshold outlines overlain. (*Right*) Colored outlines of thresholded color maps. Outlines were obtained by selecting pixels that exceeded an 80% magnitude threshold and fell within ±15° of cardinal SA, RA, or PC vectors. (Scale bar, 1 mm.) Anterior to top, medial to right. (*D*) Histograms indicate the distributions of the outlined domain diameters. (*Left*) All domains (n = 108). (*Right*) Domains separated by case. (*E*) Domain size distribution in area 3b (cf. 19). (*F*) Vector map (area indicated by rectangular box in *C Right*) thresholded to six colors. (*Inset*) Possible pinwheel centers. Note clockwise and counterclockwise SA (red), RA (green), and PC (blue) rotations.

site). Thus, our data suggest there are domains in area 1 that contain neurons with a range of response properties but whose coding function is dominated by one modality.

Vibrotactile Domain Size. We quantified the size of modality-dominant domains by thresholding and outlining the colors as shown in Fig. 2 *A–C Right*. Contours of these patches had a mean circular diameter of 192 μm (range 90–362 μm) (Fig. 2*D Left*), comparable in size with previously described anatomical and functional patches (34). These size distributions were similar across cases (Fig. 2*D Right*) [Fig. 2 *A* versus *B*, $P > 0.1$; Fig. 2 *A* versus *C*, $P > 0.1$; Fig. 2 *B* versus *C*, $P > 0.1$ (χ^2 test)].

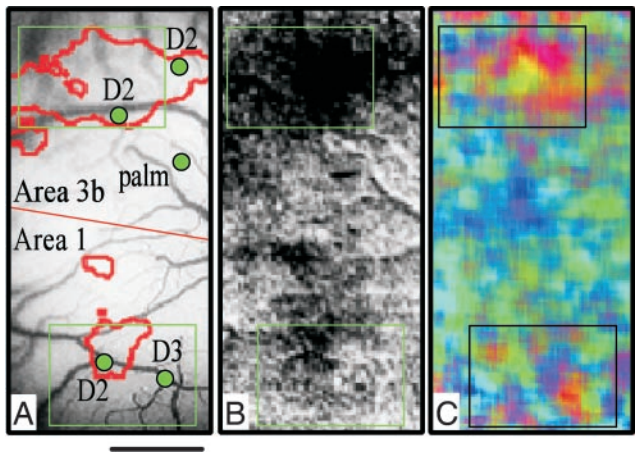

Fig. 3. D2 activation in areas 3b and 1. Green boxes indicate centers of D2 activations in area 3b (upper) and area 1 (lower). (*A*) Vessel map with recorded digit locations. (*B*) Raw image of D2 indentation. (*C*) Modality vector map (red, green, and blue indicate responses for SA, RA, and PC, respectively) shows strongest activation modules in centers of D2 activation but also weaker activation outside D2 center zones. (Scale bar, 1 mm.)

Furthermore, a similar distribution of modality-specific domain sizes is found in area 3b (Fig. 2*E*) (19, 20). Thus, these data reveal modular sizes of modality dominance in areas 3b and 1 that are comparable with the sizes of modules revealed anatomically and in studies of other sensory areas (3, 27, 32, 33, 35).

Topography of Vibrotactile Domains. Another important feature of sensory maps is the organization of the representation within a cortical area. Based on the discontinuous mapping in area V2 of color, form, and depth into well delineated stripes (3), we predicted that differential activation of three different peripheral mechanoreceptors would also map discontinuously because the three different mechananoreceptors code different attributes of a tactile stimulus: SAs encode pressure, texture, and form; RAs are sensitive to slip and motion; and PCs have the lowest thresholds to high-frequency stimulation. Contrary to our expectations, we observed in area 1 that somatosensory modality maps do not exhibit any evidence of stripe-like functional discontinuities characteristic of ocular dominance columns in area V1 or modality stripes in area V2. The distribution of pixel weights lack sudden changes in preference as seen in area V2 (e.g., strong orientation responses evidenced by saturated colors in thick/pale stripes adjacent to weak orientation responses evidenced by dark gray pixels in thin stripes). Rather, response preferences appear to vary continuously, giving rise to an appearance more reminiscent of visual orientation maps. In fact, it is interesting to note the presence of locations in the maps, which appear "pinwheel-like," rotating in clockwise or counterclockwise direction from SA (red) to RA (green) to PC (blue) dominance (Fig. 2*F*). In visual cortex, pinwheels are landmarks of orientation maps, a parameter that varies continuously (4). Whether, in area 1, these locations are true pinwheels characteristic of maps of a continuous variable or simply convergence points of discrete frequency clusters remains to be investigated.

The relationship of these modality domains to digit topography is yet unclear. However, as shown in Fig. 3, our imaging results indicate that modality-specific stimulation of a single digit extends beyond the topographic extent of the classically defined topographic map. Fig. 3*B* illustrates that a strong indentation (which activates all three receptors types) of D2 (outline of low-passed map indicated by red in Fig. 3*A*) produces millimeter-sized activations in areas 3b and 1. The response to separate pressure, flutter, and vibration stimuli exhibit activity as shown

in the vector map in Fig. 3*C*. In the vector map, the strongest responses evident inside the boxed regions correspond with the strongest activation zones in Fig. 3*B*. Pressure- (red), flutter- (green), and vibration- (blue) dominant zones are evident, consistent with examples shown in Fig. 2. However, clustered responses, although less distinct, are also evident away from the location of D2 representation (outside the boxes). These activations away from D2 are unlikely to be due to the spread of stimulation to other digits or to other parts of the hand, because under identical conditions in the same experiment, focal activations are obtained by using indentation stimuli. This nontopographic activation of SA, RA, and PC modality maps in areas 3b and 1 parallels the finding in visual cortex where complete orientation maps are imaged through stimulation of a single eye (36).

Discussion

We have shown that somatosensory cortical domains are roughly 200–300 μm in size. Our findings in area 1 strengthen the view that modularity is a common organizational feature of cortical representation. Not only have numerous anatomical and functional studies demonstrated a common patch size, on the order of 200–300 μm in diameter [in areas V1, V2, and V4; the inferior temporal cortex (37); area 7 (38); and in prefrontal areas (39)], but these anatomical patches bear close relationships to activated functional domains (e.g., ref. 40). We propose that such structure–function relationships also hold in SI and suggest the following model for our findings (Fig. 4). Single thalamocortical or corticocortical inputs in layer 4 of area 1 span several millimeters of cortex and have multiple arbors, each spanning 200–300 μm in width (33, 41). These arbors could give rise either to an array of discrete clusters or, by varying arbor overlap, continuous modality maps. In this fashion, regions dominated by single SA, RA, or PC inputs would give rise to either SA (red), RA (green), or PC (blue) domains; regions of some overlap would appear as magenta or yellow-green (not depicted); and regions of high SA, RA, and PC overlap, would appear as black or white domains (not depicted). Arbors that extend to distant nontopographic locations establish locally some degree of modality-specific dominance (compare with Fig. 3). Thus, not unlike the way horizontal isoorientation networks in V1 give rise to resulting orientation map structure, the observed maps result from overlapping horizontal networks of patchy, modality-specific dominance.

How do these maps bear on the issue of continuous and the discontinuous mapping of features in sensory cortex? The historical work of Hubel and Wiesel (42) described the discontinuous mapping of ocular dominance maps and the continuous mapping of orientation in area V1. In area V2, the modalities of color, form, and depth are organized into stripe-like domains and result in a discontinuous interleaving of three topographic maps (4). The precedence set in visual cortex led to our initial expectations that modality maps in area 1 would be similar to those found in area V2. What we found, however, is that area 1 modality maps are more reminiscent of continuous visual orientation maps (2), with no suggestion of stripe-like discontinuous mapping. Thus, despite the psychophysical and functional

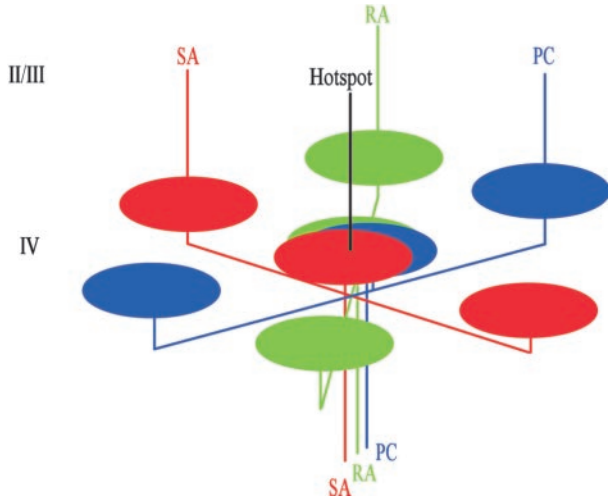

Fig. 4. Model of SA, RA, and PC preference domains in area 1. Not unlike thalamocortical arbors from the lateral geniculate nucleus, single thalamocortical or corticocortical inputs in layer 4 of area 1 have multiple arbors, each spanning 200–300 μm in width. Some arbors of each SA, RA, and PC input overlap at a ''hot spot.'' Other arbors extend to nontopographic locations away from the hot spot and locally establish some degree of modality-specific dominance. A continuous modality map results in layers 2/3 (upward lines) by varying arbor overlap: little overlap (centers of red, green, and blue domains), some overlap (e.g., magenta or yellow-green domains, not depicted), and high overlap (black or white domains, not depicted).

distinctness of the modalities of pressure, flutter, and vibration (13–15, 17, 23), there is no apparent stripe-like compartmentalization of modalities as there is in area V2. We suggest that the continuity or discontinuity of representation of a particular parameter space is indicative of ''what is important to lump together'' in a functional and psychophysical sense.

Clearly, there are differences between the representation in areas 1 and V2 that might contribute to this outcome. These potential differences include those in the hierarchy of computed parameters (e.g., area V2 is dominated by computed features such as higher order orientation, hue, and ocular disparity, whereas area 1 to some degree may still reflect the vibrotactile properties of peripheral mechanoreceptors), in the number of parameters represented (43), and in the degree of integration between different featural modalities. A major determinant in cortical functional architecture is the nature of visual and tactile stimuli themselves. In this case, the relative balance of color, form, and depth versus pressure, flutter, and vibration in natural stimuli could contribute significantly to resulting patterns of segregation (44). We suggest the architecture of cortical functional organization results in part from the demands of sensory specific perceptual processing.

We thank B. M. Ramsden and F. L. Healy for their assistance and R. H. LaMotte for use of equipment. This work was supported by the Whitehall Foundation, the Packard Foundation, the Brown–Coxe Foundation, and National Institutes of Health Grant RO1 NS044375.

1. Livingstone, M. S. & Hubel, D. H. (1984) *J. Neurosci.* **4,** 309–356.
2. Bonhoeffer, T. & Grinvald, A. (1991) *Nature* **353,** 429–431.
3. Hubel, D. H. & Livingstone, M. S. (1987) *J. Neurosci.* **7,** 3378–3415.
4. Roe, A. W. & Ts'o, D. Y. (1995) *J. Neurosci.* **15,** 3689–3715.
5. Mountcastle, V. B., Talbot, W. H., Sakata, H. & Hyvarinen, J. (1969) *J. Neurophysiol.* **32,** 452–484.
6. Pruett, J. R., Jr., Sinclair, R. J. & Burton, H. (2001) *J. Neurophysiol.* **86,** 2069–2080.
7. Costanzo, R. M. & Gardner, E. P. (1980) *J. Neurophysiol.* **43,** 1319–1351.
8. Iwamura, Y., Tanaka, M., Sakamoto, M. & Hikosaka, O. (1993) *Exp. Brain Res.* **92,** 360–368.
9. Romo, R., Hernandez, A. & Zainos, A. (2004) *Neuron* **41,** 165–173.
10. Hsiao, S. S., Lane, J. & Fitzgerald, P. (2002) *Behav. Brain Res.* **135,** 93–103.
11. Meftah, E.-M., Shenasa, J. & Chapman, C. E. (2002) *J. Neurophysiol.* **88,** 3133–3149.
12. Essick, G. K. & Whitsel, B. L. (1993) *Somatosens. Res.* **10,** 97–113.
13. Bolanowski, S. J., Jr., Gescheider, G. A., Verrillo, R. T. & Checkosky, C. M. (1988) *J. Acoust. Soc. Am.* **84,** 1680–1694.
14. Gescheider, G. A., Bolanowski, S. J., Pope, J. V. & Verrillo, R. T. (2002) *Somatosens. Res.* **19,** 114–124.
15. Mountcastle, V. B., LaMotte, R. H. & Carli, G. (1972) *J. Neurophysiol.* **35,** 122–136.

16. Johnson, K. O., Yoshioka, T. & Vega-Bermudez, F. (2000) *J. Clin. Neurophysiol.* **17,** 539–558.
17. Torebjork, H. E., Vallbo, A. B. & Ochoa, J. L. (1987) *Brain* **110,** 1509–1529.
18. Dykes, R. W., Sur, M., Merzenich, M. M., Kaas, J. H. & Nelson, R. J. (1981) *Neuroscience* **6,** 1687–1692.
19. Chen, L. M., Friedman, R. M., Ramsden, B. M., LaMotte, R. H. & Roe, A. W. (2001) *J. Neurophysiol.* **86,** 3011–3029.
20. Sur, M., Wall, J. T. & Kaas, J. H. (1984) *J. Neurophysiol.* **51,** 724–744.
21. Paul, R. L., Merzenich, M. M. & Goodman, H. (1972) *Brain Res.* **36,** 229–249.
22. Sretavan, D. & Dykes, R. W. (1983) *J. Comp. Neurol.* **213,** 381–398.
23. Romo, R., Hernandez, A., Zainos, A., Brody, C. D. & Lemus, L. (2000) *Neuron* **26,** 273–278.
24. Nii, Y., Uematsu, S., Lesser, R. P. & Gordon, B. (1996) *Neurology* **46,** 360–367.
25. Harris, J. A., Harris, I. M. & Diamond, M. E. (2001) *J. Neurosci.* **21,** 1056–1061.
26. Garraghty, P. E., Florence, S. L. & Kaas, J. H. (1990) *Brain Res.* **528,** 165–169.
27. Burton, H. & Fabri, M. (1995) *J. Comp. Neurol.* **15,** 508–538.
28. Kaas, J. H. (1983) *Physiol. Rev.* **63,** 206–231.
29. Cohen, R. H. & Vierck, C. J. (1993) *Exp. Brain Res.* **94,** 105–119.
30. Bonhoeffer, T. & Grinvald, A. (1996) in *Brain Mapping: The Methods*, eds. Toga, A. W. & Mazziotta, J. C. (Academic, London), pp. 55–97.
31. Roe, A. W. (2003) in *The Primate Visual System*, eds. Kaas, J. & Collins, C. (CRC, New York), pp. 109–138.
32. Juliano, S. L., Friedman, D. P. & Eslin, D. E. (1990) *J. Comp. Neurol.* **298,** 23–39.
33. Jones, E. G., Friedman, D. P. & Hendry, S. H. C. (1982) *J. Neurophysiol.* **48,** 545–568.
34. Mountcastle, V. B. (1979) in *The Neurosciences Fourth Study Program*, eds. Schmitt, F. O. & Worden, F. G. (MIT Press, Cambridge, MA), pp. 21–42.
35. Rockland, K. S. (1985) *J. Comp. Neurol.* **235,** 467–478.
36. Blasdel, G. G. (1992) *J. Neurosci.* **12,** 3115–3138.
37. Tsunoda, K., Yamane, Y., Nishizaki, M. & Tanifuji, M. (2001) *Nat. Neurosci.* **4,** 832–838.
38. Siegel, R. M., Raffi, M., Phinney, R. E., Turner, J. A. & Jando, G. (2003) *J. Neurophysiol.* **90,** 1279–1294.
39. Kritzer, M. F. & Goldman-Rakic, P. S. (1995) *J. Comp. Neurol.* **359,** 131–143.
40. Malach, R., Amir, Y., Harel, M. & Grinvald, A. (1993) *Proc. Natl. Acad. Sci. USA* **90,** 10469–10473.
41. Garraghty, P. E. & Sur, M. (1990) *J. Comp. Neurol.* **294,** 583–593.
42. Hubel, D. H. & Wiesel, T. N. (1977) *Proc. R. Soc. London Ser. B* **198,** 1–59.
43. Swindale, N. V. (2000) *Cereb. Cortex* **10,** 633–643.
44. Purves, D., Lotto, R. B., Williams, S. M., Nundy, S. & Yang, Z. (2001) *Proc. R. Soc. London Ser. B* **356,** 285–297.
45. Sur, M., Nelson, R. J. & Kaas, J. H. (1982) *J. Comp. Neurol.* **211,** 177–192.